PROCEEDINGS, 51st Workshop on Geothermal Reservoir Engineering
Stanford University, Stanford, California, February 9-11, 2026
SGP-TR-230

System Modeling for Optimized Operation of Large-Scale Aquifer Thermal Energy Storage-Ground Source Heat Pump System in Sweden

Mohammad Abuasbeh, Federico Antonio Castillo Burns, Björn Palm

Royal Institute of Technology (KTH), Department of Energy Technology, 10044 Stockholm, Sweden

abuasbeh@kth.se

Keywords: Aquifer Thermal Energy Storage, Ground Source Heat Pump, Long Term Performance Analysis, Shallow Geothermal Energy

ABSTRACT

This study proposes a component-based model of a heating and cooling system comprised of an Aquifer Thermal Energy Storage (ATES) and a heat pump system for a commercial building, developed using Open Modelica. The heating system is divided into the following sub-models: water-to-water heat pump, ATES system, building load, chiller, domestic hot water, and control panel. The present study simulates four operating scenarios under identical loads and boundary conditions in order to evaluate the limits of both constrained and unconstrained aquifer extraction temperatures, as well as different Heat Pump (HP) to district heating energy ratios (60/40% and 90/10%) for heating supply. Across the four scenarios, the ATES supplied between 29–50% of the annual heating load and 41–57% of the annual cooling demand. However, performance proved highly sensitive to the ATES energy extraction/injection ratio. In the unconstrained 60/40% scenario, the imbalance led to an extracted-to-injected ratio of 0.74 and increases of 69% and 21% in the pumped volume per unit of heating and cooling energy, respectively, compared to the 90/10% cases. In contrast, the 90/10% scenarios achieved a balanced operation, with ratios close to 1.27–1.24 only incurring a 3% reduction in the cooling energy injected in the ATES when constraints were applied. The highest Monthly Performance Factors (MPF) were obtained in both 90/10% scenarios, achieving 4 and 55 points for heating and free cooling, considering the HP+ATES boundary level. Free cooling values in the 90/10% scenarios are 10 points higher than both 60/40% scenarios. The results also indicate that over-extracting energy in the ATES while heating is more tolerable than over-injection during cooling for long-term aquifer sustainability and system performance. System-level results further showed that mass flow modulation improved ATES-side heat exchanger effectiveness to values as high as 0.95, improving the quality of the ATES energy and reducing risks of thermal breakthrough. The model also confirmed the value of smart control strategies, and instantaneous Key Performance Indicators (KPIs), including extraction temperature thresholds and switching between free and machine cooling, reducing electricity use and pumping energy. Overall, the study demonstrates that a balanced GSHP–ATES operation with high heat pump participation can significantly reduce district heating reliance, improve efficiency, reduce the risk of thermal breakthrough, and ensure sustainable long-term operation of the ATES.

1. INTRODUCTION

The European building sector plays a significant role in energy consumption and Greenhouse Gas (GHG) emissions. Approximately 40% of the EU's final energy consumption and 36% of its emissions derive from heating and cooling, and 75% of buildings do not reach adequate energy-efficient standards (Directorate-General for Communication (European Commission), 2021), (Schiera et al., 2021).

The EU's policy, under the Energy Union and the Energy and Climate Policy Framework for 2030, aims to reduce GHG emissions by at least 40% by 2030 from 1990 levels, and increase renewable energy use. Under new regulations, public and non-residential buildings are required to undergo renovations to improve their energy performance. By 2027, buildings must achieve a minimum score of level F, and by 2030, level E is required. Residential buildings are required to upgrade their energy performance from a minimum energy rating of G to F by 2030, and to level E by 2033 (European Commission, 2021). The EU has set even more ambitious long-term targets where a Net Zero emissions target set to 2050.

These targets emphasize the EU's urgent need to transition to energy-efficient buildings and achieve sustainable, secure, and decarbonized energy systems. Current policies and government goals greatly promote innovative solutions, especially in systems that target energy efficiency in buildings.

To meet the ambitious decarbonization goals, innovative solutions are required to increase renewable energy penetration in the building sector. Among such technologies, Seasonal Thermal Energy Storage (STES) and Heat Pump (HP) systems stand out for their potential to increase the flexibility of renewable energy as well as bridge the gap between demand and variable renewable energy production (Hesaraki et al., 2015). STES technologies—including Borehole Thermal Energy Storage (BTES) and Aquifer Thermal Energy Storage (ATES)—can store thermal energy during periods of low demand and discharge it during peak needs, smoothing out seasonal imbalances and improving system flexibility. These systems are especially effective when integrated with heat pumps, which use electricity to move and upgrade low-grade heat to useful temperatures, often delivering multiple units of heat per unit of electricity. This ratio of heat output to electrical input is referred to as the Coefficient of Performance (COP). STES can also increase the utilization of various renewable sources and mitigate renewable curtailment and waste heat, especially at the district level, making them central components of future smart energy systems.

While the integration of STES and HP systems can improve energy efficiency and support decarbonization efforts, their long-term effectiveness depends on control strategies that regulate the interaction between energy demand, storage, and supply. An improper balance—particularly in ATES systems—can reduce the long-term capacity of the aquifer to store and deliver thermal energy at the desired temperature (*Analysis of an Integrated Heating and Cooling System for a Building Complex with Focus on Long–Term Thermal Storage*, n.d.). Moreover, excessive heating over extended periods may cause undesired geochemical or ecological changes, even though the geological structure itself remains largely unaffected. Therefore, the design and operation of control systems must ensure both performance optimization and the sustainable use of subsurface resources (Lyden et al., 2022).

The digitalization of Heating Cooling and Air Conditioning (HVAC) systems through sensor networks and smart monitoring platforms presents new opportunities for improving operational efficiency and reducing maintenance costs. By capturing the main system dynamics (temperature, flow, and pressure), large volumes of operational data can be collected, enabling real-time performance tracking and fault detection. Data analytics and machine learning techniques can further be applied to predict energy consumption patterns, optimize component scheduling, and identify opportunities for retrofitting or control improvements.

Operational data can also be used to tune system models or digital twins that can aid in assessing the feasibility, performance, and scalability of innovative energy solutions without disrupting real-time operations. Through dynamic simulation environments such as TRNSYS, EnergyPlus, or OMEdit, researchers can evaluate different operating scenarios, equipment configurations, and control strategies before physical implementation. Modelling, with tools such as COMSOL or FEFLOW, enables accurate representation of thermal dynamics and allows system optimization, risk mitigation, and informed decision-making (Lyden et al., 2022).

This study aims to test the instantaneous KPIs proposed by (Abuasbeh et al., 2021a) and optimized control strategies used to improve the operation of an ATES-GSHP system used for heating and cooling of commercial office buildings by means of modelling with Open Modelica. The model includes key components such as an ATES, HP, heat exchangers, thermal loads, and displays the capability of operating under different regimes. The proposed model will allow testing of control strategies, optimization of energy use, and improvement of long-term aquifer sustainability. The model allows the evaluation of performance across a range of operating scenarios and control strategies.

2. DESCRIPTION OF THE INSTALLATION

The study area is located in the northern part of Stockholm, at the north-western side of Lake Brunnsviken, by the E4 highway (see Figure 1). The ATES system is positioned on the Stockholm esker in a property that consists of two office buildings with a total heated area of approximately 18,000 m2. The ATES system is connected to two Carrier heat pumps with a total cooling capacity of around 1.5 MW. The ATES consists of four warm wells in the northern side of the property (BV01-04 in fig 1), one of which is not currently used, and two cold wells in the south of the property (BK01-02 in fig 1). The ATES has been in operation since autumn 2016. The allowed pumping flow rate for both extraction and injection of groundwater is up to 50 l/s. The estimated saturated thickness of the aquifer ranges between 20m near the cold side and 7.5m on the warm side. The estimated distance between the center of the cold wells and the warm wells groups' centers is 90 m.

Figure 1: Image showing the esker passing through the property (left) and a zoomed-in image showing the two buildings and the ATES wells (right).

The buildings consider a centralized HVAC system designed to provide energy-efficient heating and cooling services throughout the year, with a target Energy Usage Intensity (EUI) of 50 kWh/m²/year. This system uses a GSHP and leverages its geographical proximity to an esker seen in Figure 2, allowing to utilize ground water by means of an ATES system. The combined ATES and HP units provide the buildings with a lower EUI for heating and cooling services. The system harnesses geothermal energy that provides a reliable source for the heat pump, extracting and storing energy from the water in the form of sensible heat. The hot and cold wells are charged and discharged seasonally, depending on the needs of the buildings.

2.1 Heating and cooling system operation modes

Heating: during which the heat pumps are used to supply heating to the building heating distribution network and domestic hot water while using district heating as a backup. On the heat pump evaporator side, the heat source is being divided between the ATES and the building cooling distribution network. This means that while heating, the heat pump is simultaneously cooling the building as well.

Free cooling: during which the ATES provides direct cooling (without the use of the heat pumps) towards the building cooling distribution network, and domestic hot water demand is supplied using district heating.

Machine cooling: during which the heat pumps are used to supply cooling to the building cooling distribution network and domestic hot water demand, usually supplied by the heat pumps' condenser while using district heating as a backup. The excess heat from the condenser is rejected to the air chillers on the roof. This means that during machine cooling, there will be some form of heating as well.

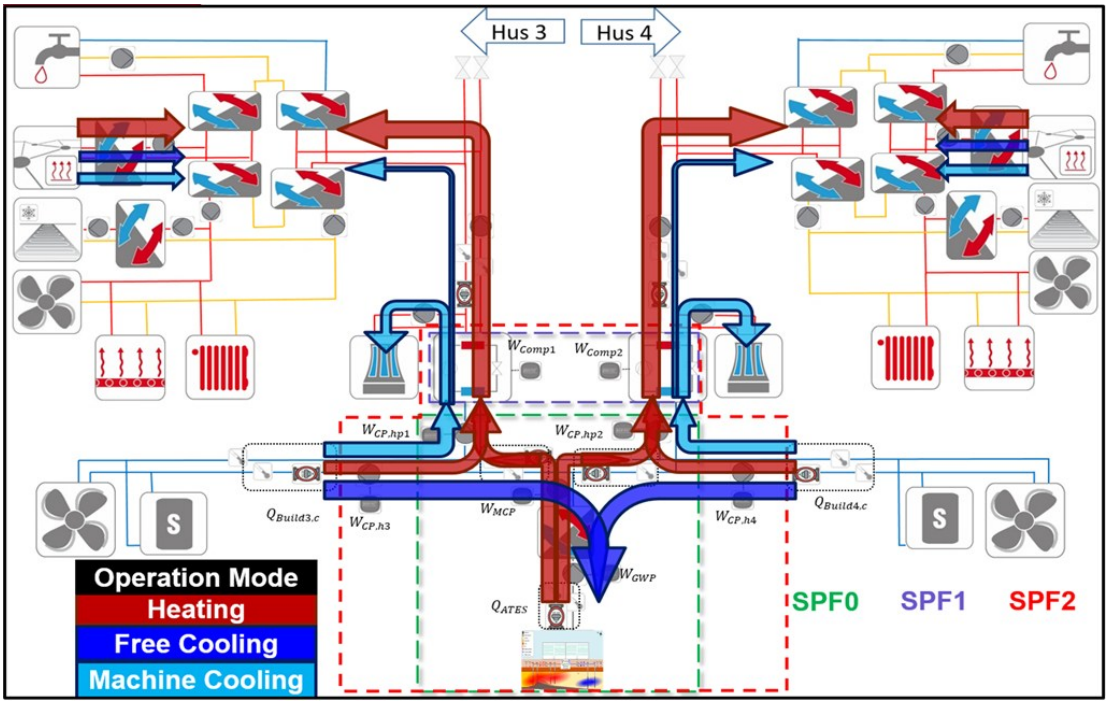

Figure 2: Schematic of the heating and cooling system in Solna with the boundary levels for SPF0-SPF2 showing the energy flow in each of the main operation conditions, heating (red arrow), free cooling (dark blue arrow), and machine cooling (light blue arrow). The ATES location in the system is represented by the small schematic at the bottom part of the figure (Abuasbeh, 2021; Spitler et al., 2021)**.**

3. SYSTEM KEY PERFORMANCE INDICATORS DEFINITION

To evaluate the heating and cooling system, we will use the seasonal performance factor (SPF) or the monthly performance factor (MPF) as the main key performance indicator. SPF is defined by the following equation.

$$SPF = \frac{\sum Q_{thermal}}{\sum W_{electrical}} \quad (1)$$

Where $Q_{thermal}$ is the thermal energy utilized for heating or cooling during the season (usually a year), and $W_{electrical}$ is the electrical energy consumed in order to deliver the heating or cooling demand during that period of time.

Each of the boundary levels describes a certain group of components of the system. SPF_0, SPF_1, and SPF_2 are the ATES, heat pump circuits, and the combined ATES-GSHP loop, respectively, as shown in Figure 2. The subscripts (c) and (H) indicate cooling and heating operation respectively. The *SPFs* are defined by the following equations

$$SPF_{C0} = \frac{Q_{ATES,c}}{W_{GWP,fcm} + W_{MCP,fcm} + W_{CP,hp}} \quad , \quad SPF_{H0} = \frac{Q_{ATES,h}}{W_{GWP,hm} + W_{MCP,hm} + W_{CP,\mathrm{hp}}} \quad (2), (3)$$

$$SPF_{C1} = \frac{Q_{Evap}}{W_{Comp}} \quad , \quad SPF_{H1} = \frac{Q_{Evap}}{W_{Comp}} \quad (4), (5)$$

$$SPF_{C2} = \frac{Q_{Build,c}}{W_{GWP,fcm} + W_{MCP,fcm} + W_{CP,hp,mcm} + W_{Comp,c}} \quad , \quad SPF_{H2} = \frac{Q_{Cond}}{W_{GWP,hm} + W_{MCP,hm} + W_{CP,hp,hm} + W_{Comp,hm}} \quad (6), (7)$$

Where W_{GWP}, W_{MCP}, W_{CP}, W_{Comp} indicate the electrical energy consumption the ground water pumps from the Aquifer, the main circulation pump connecting the ATES to the heating system, a circulation pump, and the heat pumps compressor respectively. The

subscripts (fcm), (hm), (mcm), and (hp) indicate free cooling mode, heating mode, machine cooling mode, and heat pump related component. $\boldsymbol{Q_{ATES}}$, $\boldsymbol{Q_{Evap}}$, $\boldsymbol{Q_{Cond}}$, $\boldsymbol{Q_{Build}}$ indicate the thermal energy exchanged with the ATES, heat pump evaporator, heat pump condenser, and the building cooling network respectively as shown in Figure 2.

3.1 ATES Key Performance Indicators Definition

The heat exchanger efficiency ($\boldsymbol{\eta_{HEX}}$) proposed by (Abuasbeh et al., 2021a) describes how much of the maximum possible temperature difference across the heat exchanger has been utilized. This efficiency can be described from both points of view of the building ($\boldsymbol{\eta_{HEX_{build}}}$) or the ATES ($\boldsymbol{\eta_{HEX_{ATES}}}$). They can be formulated as the ratio between the temperature difference between the inlet and the outlet of the heat exchanger, from either the building or the ATES side, and the temperature difference between the inlets of the heat exchanger from each side, as shown in equations (8) and (9). Furthermore, the heat exchanger efficiency balance for both sides can be introduced and formulated as shown in equation (10).

$$\boldsymbol{\eta_{HEX_{build}}} = \frac{\left|T_{Build_{HEX_{Out}}} - T_{Build_{HEX_{In}}}\right|}{\left|T_{Build_{HEX_{In}}} - T_{ATES_{HEX_{In}}}\right|} \quad (8), \qquad \boldsymbol{\eta_{HEX_{ATES}}} = \frac{\left|T_{ATES_{HEX_{Out}}} - T_{ATES_{HEX_{In}}}\right|}{\left|T_{Build_{HEX_{In}}} - T_{ATES_{HEX_{In}}}\right|} \quad (9)$$

$$\boldsymbol{\beta_{HEX}} = \frac{\eta_{HEX_{build}} - \eta_{HEX_{ATES}}}{\eta_{HEX_{build}} + \eta_{HEX_{ATES}}} \quad (10), \qquad \sigma_{HEX} = \eta_{HEX_{Build}} + \eta_{HEX_{ATES}} \quad (11)$$

Where $\boldsymbol{T_{build_{HEX_{In}}}}$, $\boldsymbol{T_{build_{HEX_{Out}}}}$, $\boldsymbol{T_{ATES_{HEX_{In}}}}$ and $\boldsymbol{T_{ATES_{HEX_{Out}}}}$ are the inlet and the outlet temperatures from the main heat exchanger from the building and ATES side respectively. Ideally, the temperature difference across the heat exchanger from the building side and the ATES is desired to be as high as possible. High-temperature difference from the building side ($\Delta \boldsymbol{T_{building}}$) leads to the warmest (or coldest during summer) forward temperature during winter towards the building heating system. Similarly, a high-temperature difference from the ATES side ($\Delta \boldsymbol{T_{heating}}$ or $\Delta \boldsymbol{T_{cooling}}$) leads to the coldest (or warmest during summer) injection temperature during winter in the ATES, which improves the storage for the following season. The heat exchanger efficiency balance ($\boldsymbol{\beta_{HEX}}$) would have a value of range between 1 and -1. Where a negative value would mean that the operation over the main heat exchanger is more optimized in favor of the building system, and a positive value would mean that the operation is in favor of the ATES. These efficiencies provide insight into how optimally the system operation has been from the point of view of the ATES and building heating and cooling.

4. SYSTEM MODEL

The model's architecture and layout are based on the Rosenborg Hus 3 and Hus 4 flow diagrams shown in Figure 3. The following simplifications were considered in light of the complexity and extent of the real system:

1. Heating loads were lumped into 2 main loads: domestic hot water and space heating.
2. Cooling loads were also lumped into space cooling and base cooling.

The diagram of the real system presents a mirrored system between Hus 3 and Hus 4, Therefore, only Hus 4 was modeled. The ATES and main heat exchanger feed two separate buildings (Hus 3 and Hus 4), each with independent HPs. These units have recently been connected to allow an individual HP to supply energy to Hus 3 and 4 simultaneously, reducing the time frame where the system load does not meet the minimum HP load. Most of the model loads are lumped and do not explicitly represent ventilation and air conditioning as separate subsystems; instead, their effects are captured within the aggregated load.

Given these assumptions, the following section presents how the model was designed and implemented in OMEdit, which allows the system to be divided into individual models, which makes it easier to develop, troubleshoot, test the performance, and evaluate each model under controlled inputs. This ensures correct behavior before integration. These individual loops were then imported and connected to the main system model.

2.1 Main Loop

Figure 3 shows the layout of the Rosenberg HVAC system, where the loads and main components can be identified. To allow smoother and easier modelling, the HVAC system has been split into five main operating loops, as shown in Figure 4.

Aquifer loop: Considers the ATES hot and cold wells, piping, and valves required to invert flow direction, the building's main heat exchanger, and the building's flow reversal section used to maintain counter flow direction when changing operational modes.

Heat pump loop: The HP loop considers both source and sink loops. The source side is connected via fluid ports to the aquifer loop and the building's cooling loop. In the load side (when heating), the hot water leaving the HP goes through four heat exchangers; the flow is split into two, where one branch is for space heating and a second branch for DHW. Each branch has two heat exchangers connected in series, where the first heat exchanger delivers heat from the HP load to the DHW and space heating loops, and a second unit in series provides energy from the DH network when not enough heat is provided by the HP. This is controlled by a proportional–integral (PI) controller, which regulates a valve to adjust the flow in the DH loop. The HP circuit is also connected to the chiller loop through a HEX used during MC.

Building loop: This represents the building's load, for either heating or cooling mode. The model was constructed based on a simplified building model presented in the Buildings Library training workshop at the American Modelica conference 2024 (*Modelica Buildings*

Library Training at the American Modelica Conference, n.d.). It uses a mixing volume of air with thermal connectors and attachments. These connectors are used to represent internal heat gain, the building's thermal inertia, and the energy exchanged with the environment.

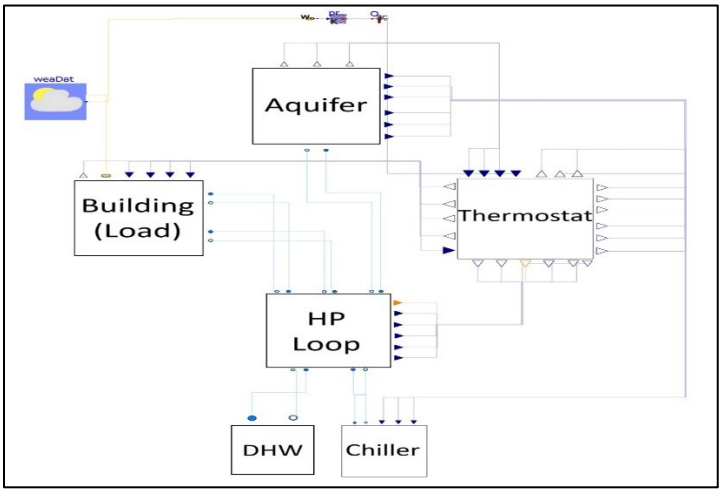

Figure 4: OMEdit system model, displays the main loops described above, input and output signal connectors (blue and white triangles), inter-model interconnections (dark blue lines), fluid input and output ports (blue and white circles), and fluid connections (light blue lines) exchange information among the individual models.

Chiller loop: The chiller loop is connected to the heat pump loop through fluid ports. The fluid exits the model to go through the heat exchanger, where it absorbs energy from the main HP loop, then returns through the fluid port towards the chiller pump. The condenser of the chiller uses air at ambient temperature, where the ambient air temperature is read from the Typical Meteorological Year (TMY) file for Stockholm. The TMY represents a statistically typical year constructed from representative months of long-term weather data. This loop is only used when the system operates in machine cooling, enabling the system to dissipate the heat rejected by the HP.

Domestic hot water loop: The DHW loop reads the hot water demand and tap water temperature from a combi table connected to data files and modulates the flow according to the given demand. This provides a dynamic load for the heating system (HP and DH unit). The fluid ports are connected to two heat exchangers, receiving energy from the HP condenser and DH loops.

Thermostat: The thermostat model reads the building's internal temperature, the ATES hot and cold well outlet temperatures, and the ambient air temperature. Based on predefined setpoints, the model uses the Boolean output of two hysteresis blocks to determine whether the heating or cooling mode is active. When heating is active, the thermostat checks if the hot well temperature exceeds the extraction threshold and whether the ambient air temperature also meets its threshold. If both conditions are satisfied, the model provides the corresponding heating control values to all components via a multi-switch block for each signal.

When cooling is active, the thermostat first decides between free cooling and machine cooling. This is determined by comparing the cold well extraction temperature to the threshold: if it is below the threshold, the Boolean variable 'free cooling' becomes true, and the system operates in free cooling mode. If the threshold is not met, machine cooling is activated instead.

The thermostat determines the correct operational mode — heating, free cooling, machine cooling, or off — with each mode linked to predefined values that are passed as output signals by the multi-switches to all sub-models and their components, such as valves, pumps, HP, chiller, and ATES. Additionally, before the pumping signals are sent to their respective block models, their value is modulated to increase or reduce the desired flow based on the inlet and outlet temperatures of the main heat exchanger, maximizing the energy quality in the ATES.

4. MODEL SCENARIOS

To evaluate the performance of the modeled system and assess the effect of different operational strategies, four scenarios were developed. These scenarios represent the current baseline where ATES extraction temperatures are unconstrained, and an ideal case where the aquifer has extraction thresholds and yearly ATES temperatures remain stable. Both cases are then simulated with 2 different proportions of energy delivered by the HP and DH network. By simulating each scenario under the same boundary conditions (ground temperature, weather data and Water demand) and load profiles, monthly and annual performance metrics such as heating and cooling loads, energy balances, and KPIs can be calculated and compared. The aim of this analysis is to understand how control strategies, load balancing, and ATES operation affect energy efficiency, seasonal balance, and system sustainability.

4.1 Scenario 1 – Unconstrained ATES 60/40%

The Unconstrained scenario represents the current operating conditions of the ATES system under permissive limits for groundwater extraction temperatures. Hot well extraction temperature is maintained above 6.5 °C, while cold well extraction temperature is kept below 13.5 °C. At the start of the simulation year (2019), both wells are in thermal balance at the undisturbed ground temperature of 10 °C. Heating demands are met through a combination of HP and DH ratio, with a 60%, and 40% ratio of heating energy, respectively. This proportion is achieved by limiting the T_(amb-HP) maximum ambient temperature the HP is permitted to be turned on and reducing the flow of the load side of the HP as described in Section 4.8. This scenario reflects the present-day proportions of load met by the systems and permissive ATES management.

4.2 Scenario 2 – Unconstrained ATES 90/10%

This scenario assumes an ideal HP/DH heating ratio, where the heat pump can meet the majority of the building's heating loads. Restrictions on HP operating conditions limited to T_amb<15 °C. District heating is used as a supplementary source mainly for domestic hot water loads. All operating conditions including permissive ATES extraction temperature limits and initial well temperatures are analogous to scenario 1.

4.3 Scenario 3 – Constrained ATES 60/40%

Scenario 3 represents a constrained ATES operation aimed at maintaining seasonal balance of the geothermal resource. The hot well extraction temperature is limited to 9.9 °C, and the cold well extraction temperature is likewise limited to 9.9 °C, ensuring seasonal thermal equilibrium in the aquifer. The heating supply is maintained at the current 60 % to 40 % HP to DH ratio. This configuration balances the ATES thermal loads over the year while preserving the present DH/HP energy contribution ratio.

4.4 Scenario 3 – Constrained ATES 60/40%

Scenario 4 applies the constrained ATES operation strategy described in Scenario 3, with hot and cold well extraction temperatures both limited to 9.9 °C to maintain seasonal thermal balance. The key difference is the heating supply distribution, which follows the 90 % / 10 % HP to DH ratio used in Scenario 2. This configuration combines the thermal sustainability of the constrained ATES approach with the high HP contribution of the unconstrained, HP-dominant case.

5. SCENARIO INPUT PARAMETERS

HP to DH proportion: to create each independent modeling scenario presented in section 4, two variables were modulated:

1. HP load loop pump speed: The input signal was reduced from 1.2 to 0.9 in scenarios 1 and 3. This reduces the load loop flow and the power delivered by the HP to the building's main heat exchanger. In turn, this creates the condition that the building supply temperature is not met by the HP heat exchanger; therefore, the DH heat exchanger connected in series is activated and provides the remaining energy to satisfy the building supply set temperature.

2. Heat pump ambient temperature cut-off: As can be seen in Figure 10 in (Abuasbeh, 2021), the HP does not operate when ambient temperatures exceed 13°C, since the partial load is too low for the minimum HP load capacity. Therefore, the DH unit covers any remaining loads. The OMEdit thermostat model incorporates such a safeguard, checking the ambient temperature before enabling heating. This setting was changed to 8 °C to reduce the contribution of the HP and to obtain the desired energy proportion for scenario 1 and scenario 3.

Aquifer temperature: In the main thermostat logic, heating and cooling modes are fitted with a safeguard that reads the ATES extraction temperature for both cold and hot wells. As seen in Figure 16, this was possible by modifying the buildings library aquifer block (model), and installing temperature sensors in the extraction point of the first control volume array of each well.

The thermostat, by means of a logic threshold block, decides if the ATES is available for heating and cooling, where each equation returns a Boolean according to the result of Equation (12) and Equation (13).

$$T_{HotWell} > T_{H,th} \quad (12) \qquad T_{ColdWell} < T_{C,th} \quad (13)$$

6. RESULTS AND DISCUSSION

The following section details the main results obtained for each modeled scenario, reviewing how the loads are met, the performance of the modeled components monthly, and seasonal indicators that characterize the system and the main heat exchanger performance.

6.1 Scenario 1 Unconstrained ATES 60/40%

The building: the total simulated monthly heating and cooling load for the Rosenborg Hus 4 Building is presented in Figure 5. The maximum heating load of 55 MWh occurs in January, while the maximum cooling load of 37 MWh is reached in July. The pattern of demand remains stable over the four simulated years, as the TMY weather file is identical for each year. These results do not show machine cooling, as free cooling is sufficient to cover all demands. This is possible because the ATES extraction temperature is unconstrained.

Almost all DHW demand is supplied by the DH system. This can be explained by two main factors: first, DHW demand is relatively constant throughout the day, while the HP operates in cycles of 30–45 minutes and is not activated for such loads; second, the HP loop is unable to reach the DHW setpoint temperature. Consequently, the DH system is required to raise the water temperature from 45 °C (HP

outlet) to the DHW setpoint of 50 °C, even if the HP happens to be in operation during the load. Finally, in the summer months, the DH unit provides the total heating load. This is due both to the restriction on HP operation above 15°C ambient temperature and to the very low building space heating demand during this period.

ATES: Contrary to what is seen in Figure 5 (left), the overall energy expenditure of the ATES is greater for cooling loads than for heating loads, with a steady profile throughout the four-year simulation. Figure 5 (right) reveals the imbalances caused by the reduced energy share provided by the HP: in summer, the total cooling load is injected into the ATES; however, in winter, only 60% of the heating energy is extracted from the hot well.

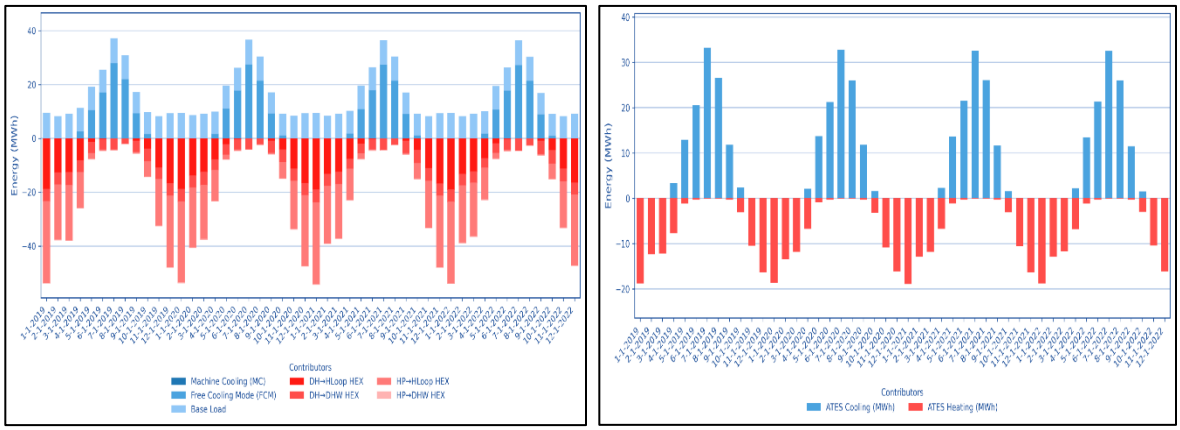

Figure 5: Building monthly cooling and heating loads by source for unconstrained ATES with 60/40% energy distribution (left). Monthly energy extracted and injected from the ATES [MWh] for cooling and heating. Scenario with unconstrained aquifer and 60/40% energy distribution (right).

These imbalances can be clearly seen where 110 MWh are used for cooling, and only 75 MWh are extracted for heating during 2019. This trend is mostly maintained during the remaining 3 years of simulation, only with a small 2 MWh reduction from the cooling loads. Note that the energy balance for the ATES is considered positive when injecting energy into the ATES (during heating season) and negative when extracting energy during the cooling season.

It is important to note that some of the energy for the base cooling load is not accounted for in this plot, as the flow used for the base cooling during the heating season is recirculated from the outlet of the HP, and does not involve the ATES (this flow can be seen in Figure 2, where the HP outlet water is split between the recirculation loop and the main HEX).

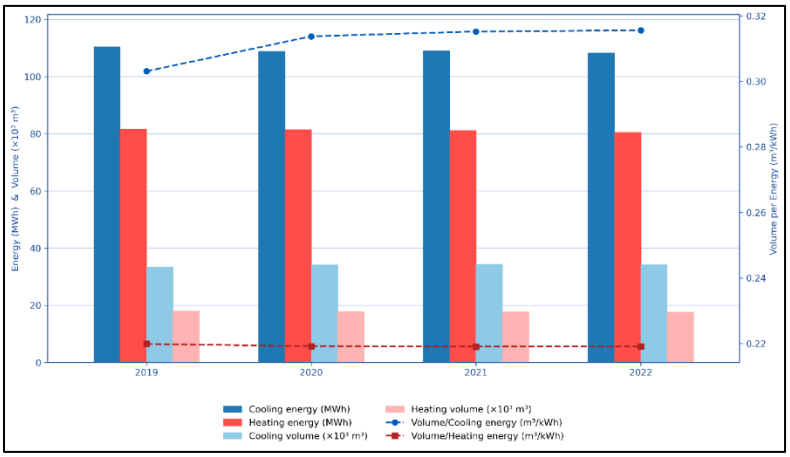

Figure 6: Total ATES yearly energy [MWh] and cooling/heating water volume [10e3 m3] (left axis) and volume per unit of energy [m3/kWh] (right axis) for Unconstrained ATES with 60/40% energy distribution.

Figure 6 illustrates a growing trend in the cooling water volume required per unit of delivered energy, highlighting the effects of the unbalanced ATES system. Each year, an increasing volume of cold water must be extracted from the ATES to satisfy the same cooling demand. This is represented by the dotted blue line: in 2019, approximately 0.3 m³ of cold water was required per 1 kWh of cooling energy, while by the end of the simulation, this value had risen to nearly 0.34 m³/kWh.

In contrast, the volume extracted from the hot well remains comparatively stable, although a slight decreasing trend can be observed over the simulation period. It is important to note that despite these changes in specific water volumes, both the total heating and cooling

volumes, as well as the overall energy extracted from the ATES, remain nearly constant over the four simulated years. This suggests that the ATES imbalance primarily affects the efficiency of cold well utilization, while the hot well efficiency operation only slightly increases, requiring a smaller volume of water.

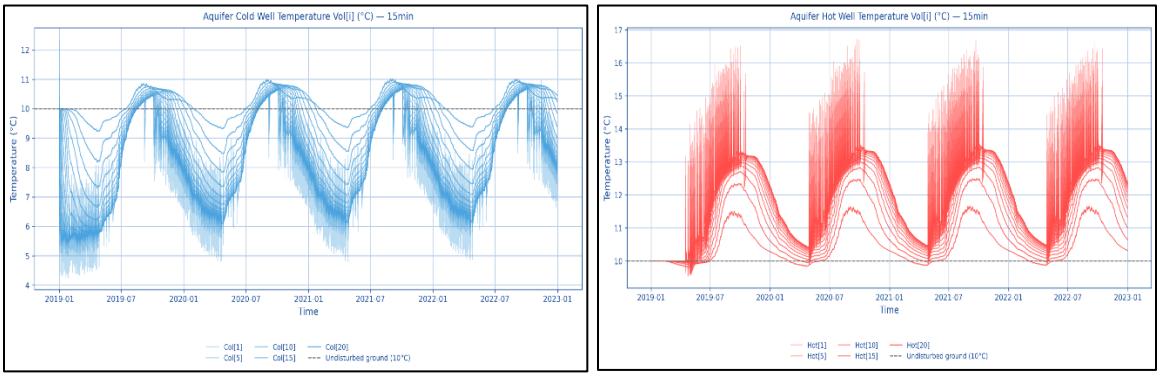

Figure 7: Aquifer water temperature distribution for each one of 20 control volumes of the ATES model in scenario 1. The cold well temperature distribution can be seen in (left), and the hot well temperature distribution is depicted in (right). Both plots consider 15-minute time series intervals.

The extraction and injection temperature profiles of the ATES system can be seen in Figure 7 (left)-(right), providing further insight into the thermal dynamics of the ATES wells under the simulated scenario. The cold well injection temperature remains consistently low in the first cooling season, with values between 3 and 7.5°C. Through the remaining simulation, injection values rise, reaching up to 10 °C. When analyzing the hot wells, injection temperature shows greater variability, starting low at nearly 10°C early in the cooling season and rising to approximately 16.5 °C towards the end.

Extraction temperatures can be distinguished as a steady upward curve in Figure 7 (left) and a steady downward curve in Figure 7 (right), for the cold and hot wells, respectively. The cold wells extraction temperatures degrade over the simulation years, reaching nearly 11°C at the end of the cooling season of the 4th simulated year. Notably, the cold well injection temperatures are lower than those reported in the real building study (Abuasbeh et al., 2021b). This difference can be attributed to adequate mass flow modulation on the ATES side, which maximizes the available ΔT of the main HEX.

A small but steady temperature increase can be observed in the cold well over the four years of simulation. This is in contrast with the case study (base scenario presented by (Abuasbeh, 2021) in Figures 15 and 16), where a much sharper rise in extraction temperature has been documented, where cold well extraction reaches 13 °C in the third year of operation. The ability of the model to limit the cold well temperature rise highlights the positive effect of ATES mass flow modulation, improving the quality of the thermal energy stored and reducing long-term degradation effects of the hot and cold wells. Nonetheless, even under these favorable conditions, a net heating effect on the cold well is observed.

This unconstrained scenario represents the most challenging case for the ATES, since it assumes relatively low HP participation—implying higher reliance on the DH system—and allows unconstrained extraction temperatures from the wells. Despite these assumptions, the results demonstrate how modulation mitigates some of the critical effects associated with ATES imbalance.

ATES mass flow modulation is key in preserving ATES energy quality and the temperature difference (ΔTbetween extraction and injection. When operating at a lower ΔT, a larger volume of water is required for a given amount of extracted energy, which increases advective transport from the hot well to the cold well. This phenomenon is called thermal breakthrough and pushes warmer water into the cold well, accelerating its thermal degradation. Minimizing advective effects is crucial for maintaining high thermal storage efficiency. This is directly related to ATES mass flow modulation, which enables ΔT to be maximized during operation.

These results underscore that the ATES mass flow modulation enables the same amount of energy and power to be delivered at higher ΔT, effectively minimizing advective effects and ensuring more sustainable long-term operation of the thermal storage system.

KPI evaluation: Figure 8 (left) shows the results for the MPF of boundary level 2, where most of the pumps are accounted for in the calculations. The figure shows a significant difference between the heating and free cooling values; this is primarily because heating requires the work of the HP compressor, which uses a substantial amount of energy, lowering the performance values. Free cooling is therefore preferred to machine cooling in the real scenario, as the energy required to obtain a unit of cooling is nearly one-tenth of the machine cooling values. This can be seen in the constrained scenarios where machine cooling is forced due to limitations in the extraction temperature of the ATES's cold well. The results indicate a small but consistent reduction in cooling performance over the simulated period. However, its value declines within the same season due to progressive degradation of the ATES cold well temperature. An annual downward trend is also observed across the subsequent years of simulation, confirming the cumulative effect of cold well heating on cooling efficiency. By contrast, the heating performance index remains relatively stable throughout the four-year period, suggesting that heating operation is less sensitive to the gradual thermal imbalance of the storage system.

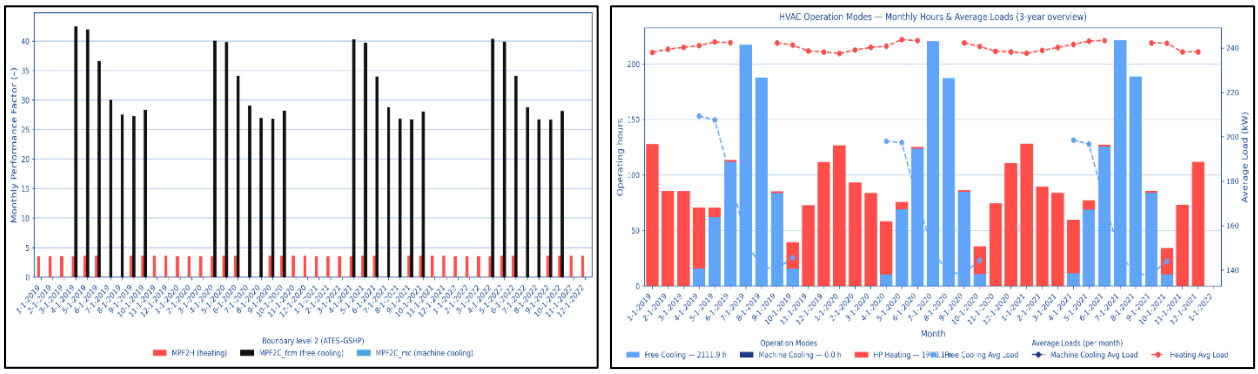

Figure 8: MPF for Boundary level 2, which accounts for both ATES and HP units and their respective circulation pumps for the Unconstrained ATES with 60/40% energy distribution (left), and operating hours and heating-cooling power for each operating mode for the Unconstrained ATES with 60/40% energy distribution (right).

The results show that the free cooling mode requires longer operating cycles and a higher number of monthly hours compared to heating, even though the previously presented heating loads are of greater magnitude. This apparent discrepancy can be explained by the difference in power delivered to the building, shown on the secondary axis of Figure 8 (right). While the heat pump is able to deliver higher power output during heating operation, the free cooling mode provides lower power, thus requiring longer operating hours to satisfy the same load. This effect can be directly linked to the ATES mass flow modulation. By reducing the groundwater flow rate, the modulation maximizes the temperature difference (ΔT) across the main heat exchanger, improving ATES charging and discharging efficiency. However, this comes at the expense of reduced instantaneous power delivery, which in turn extends the cycle duration and increases total operating hours in free cooling mode.

6.2 Scenario 2 Unconstrained ATES 90/10%

The Building: Figure 9 (left) presents the monthly building cooling and heating loads by source, for the unconstrained ATES case with a 90/10% HP/DH energy distribution. Using the same building loads and boundary conditions as scenario 1, shifting to this 90/10% distribution noticeably reduces DH contributions while meeting the same demand. The analysis also reveals a persistent mismatch between heat pump operation and DHW demand. Implementing a hot water storage tank on the load side of the HP loop could decouple production from demand and buffer thermal energy, enabling a much higher HP share in DHW, thereby further decreasing reliance on DH.

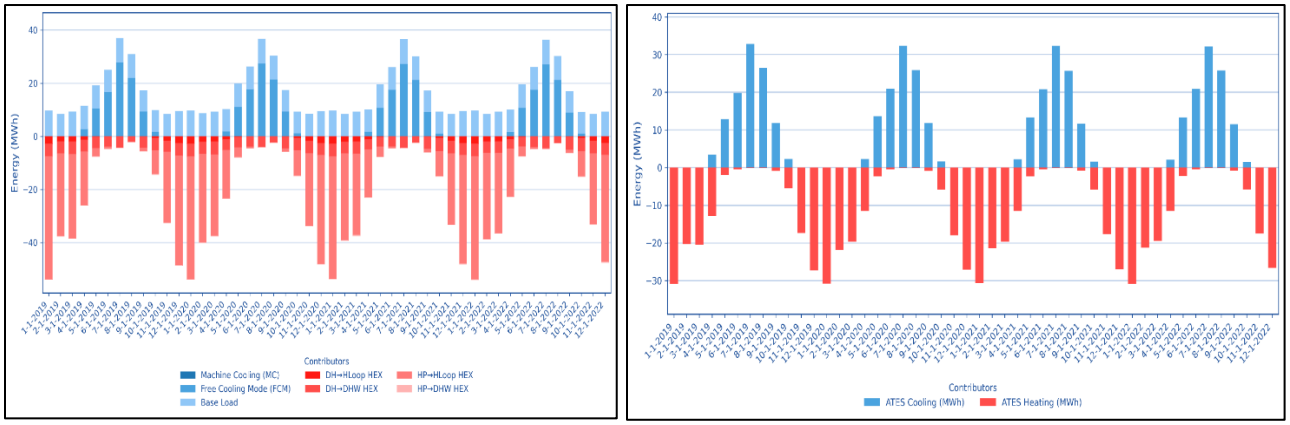

Figure 9: Building monthly cooling and heating loads by source for unconstrained ATES with 90/10% energy distribution (left). Monthly energy extracted and injected from the ATES [MWh] for cooling and heating. Scenario with unconstrained aquifer and 90/10% energy distribution (right).

The ATES: Figure 9 (right) shows a more balanced ATES operation compared to scenario 1, with the HP supplying about 90% of the heating load. The annual ATES energy exchange is shifting towards balance, with an extracted-to-injected energy ratio of approximately 0.8. This means that the extracted energy represents nearly 80% of the injected amount, indicating a smaller imbalance and a more favorable equilibrium in the aquifer. As more energy is extracted than injected, the ATES shows a net cooling effect, evident in the cold well's annual net volume and in the water volume required per unit of energy when operating in free cooling. Compared with Scenario 1, the water volume per unit energy is lower for both cooling and heating: the cold-well specific volume drops by 17.5%, and the hot-well specific volume drops by 13.4%. These reductions indicate improved hydraulic efficiency for the pumps and less ATES throughput to deliver the same thermal services.

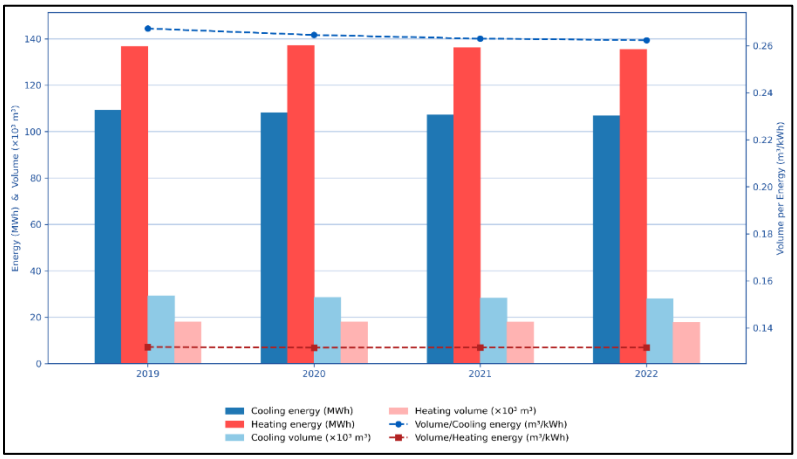

Figure 10: Total ATES yearly energy [MWh] and cooling/heating water volume [10e3 m3] (left axis) and volume per unit of energy [m3/kWh] (right axis) for Unconstrained ATES with 90/10% energy distribution.

The ATES hot and cold well temperature distributions remain stable across all four simulated years. Despite the unconstrained operation, hot well extraction temperatures consistently stay above 10 °C and below 10 °C in the cold well, suggesting that explicit extraction-temperature constraints may be unnecessary when the system is properly balanced. Notably, the cold-well injection temperatures are very low (≈ 2–5 °C), which supports efficient free cooling but warrants attention to long-term thermal breakthrough and any regulatory minimum temperature limits. Injection temperatures in the hot well are also low at the beginning of the cooling season, reaching a minimum of 7°C.

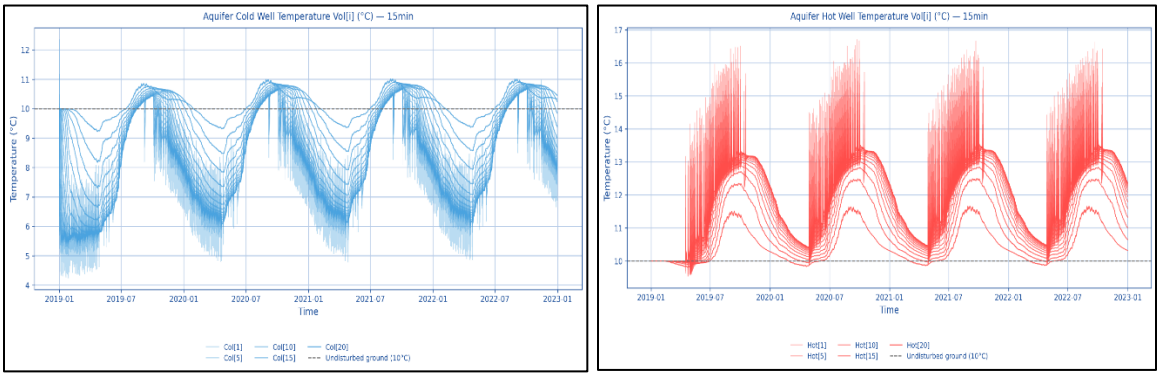

Figure 11: Aquifer water temperature distribution for each one of 20-control volume of the ATES modeled in Scenario 2. The cold well temperature distribution can be seen in (left), and the hot well temperature distribution is depicted in (right). Both plots consider 15-minute time series intervals.

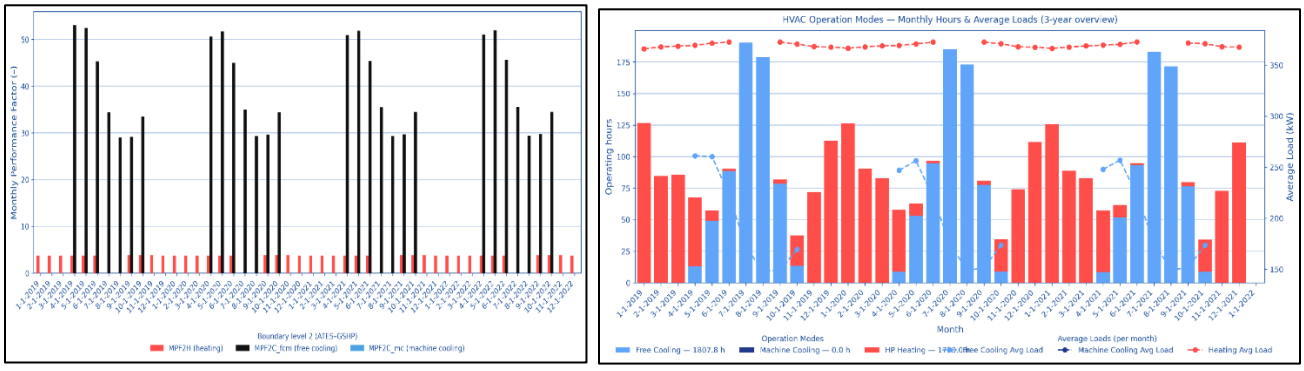

Figure 12: MPF for Boundary level 2, which accounts for both ATES and HP units and their respective circulation pumps for the Unconstrained ATES with 90/10% energy distribution (left), and operating hours and heating-cooling power for each operating mode for the Unconstrained ATES with 90/10% energy distribution (right).

KPI evaluation: the ATES MPF index improves significantly when moving from Scenario 1 to a more balanced ATES case. Whereas in Scenario 1 the MPF peaks at $MPF_{0C} \approx 42$ and $MPF_{0H} \approx 18$, the balanced scenario delivers 10 points higher performance in both cooling

and heating. This consistent increase exposes how a thermally balanced ATES (i.e., closer match of extracted vs. injected energy) improves system performance by sustaining larger usable temperature differences and reducing aquifer throughput, significantly raising the performance in both operating modes. This improvement is linked to the reduced volume of water required per unit of energy exchanged: less volume means lower pumping energy, which in turn results in a higher indicator value. The operating hours shown in Figure 12 (right) are significantly lower than scenario 1, with around 30 h reduction in monthly free cooling values for the peak months, while heating operating hours remain constant. The average heating and cooling power is significantly lower than that of scenario 1.

6.3 Scenario 3 constrained ATES 60/40%

The Building: the initial 60/40% scenario is the first to demonstrate machine cooling, which is consistently observed from August to October in each simulated year. This finding indicates that a reduction in the ATES heating energy share from 90% to 60% results in a hotter cold well and more elevated extraction temperatures that exceed the undisturbed threshold of 10°C; the system is forced to operate in the alternate cooling method (machine cooling). The monthly load and energy distribution can be seen in Figure 13 (left). The ATES energy injection in the cooling cycle is cut short when the threshold is reached. Figure 13 (right) shows that free cooling is cut to near zero in September and October.

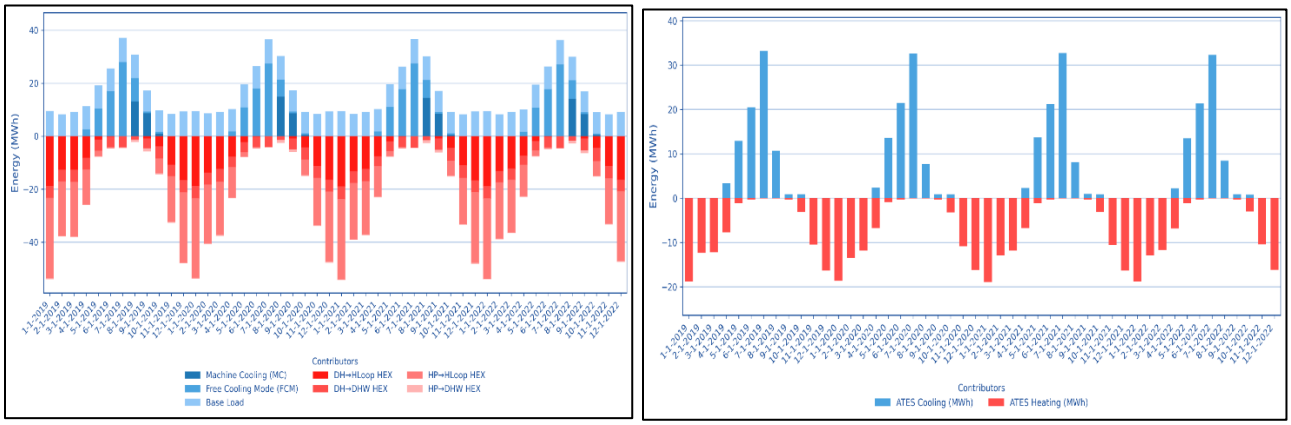

Figure 13: Building monthly cooling and heating loads by source for constrained ATES with 60/40% energy distribution (left). Monthly energy extracted and injected from the ATES [MWh] for cooling and heating. Scenario with a constrained aquifer and 60/40% energy distribution (right).

The ATES: the yearly ATES energy balance for the constrained 60/40% scenario, this is the only scenario that displays a nearly 1 to 1 energy ratio in the ATES (extraction vs injection).

In terms of the ATES performance, the volume per unit of energy is similar to scenario 1 (Figure 14), but with an 8% reduction during free cooling, showing that when comparing both 60/40% scenarios, a better thermal free cooling performance can be observed when the cold well is maintained under 10°C. However, the economic aspects should also be considered when integrally assessing the system. This is beyond the scope of this study, but could result in interesting findings for the case study, given that the energy distribution of this scenario is closely related to the case study's current operating conditions.

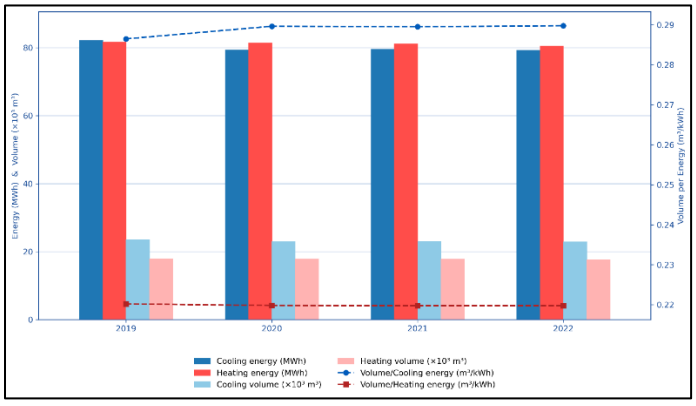

Figure 14: Total ATES yearly energy [MWh] and cooling/heating water volume [10e3 m3] (left axis) and volume per unit of energy [m3/kWh] (right axis) for constrained ATES with 60/40% energy distribution.

The temperature distribution, in Figure 15, depicts a stable behavior for the hot and cold wells through the simulation, with extraction and injection temperatures very similar to scenario 1 (unconstrained 60/40%), the main difference being that the maximum seasonal cold well extraction temperature in scenario 1 is 10.6°C, while in scenario 3 it is limited to 9.9 °C.

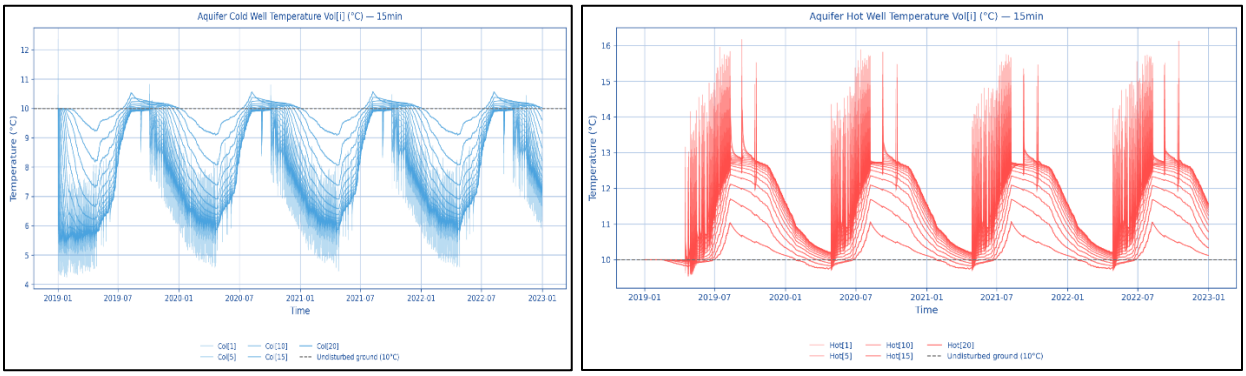

Figure 15: Aquifer water temperature distribution for each one of 20-control volume of the ATES modeled in Scenario 3. The cold well temperature distribution can be seen in (left), and the hot well temperature distribution is depicted in (right). Both plots consider 15-minute time series intervals.

KPI Evaluation: As illustrated in Figure 16 (left), the monthly performance of the ATES closely resembles scenario 1, with only minor variations in values during the final three months of the cooling season. In this scenario, MC is activated, leading to intervention in the overemployment of the cold well. The consequence of this is elevated monthly performance indices during the period spanning August to October. The figure also indicates a performance level about 10 points lower than in the scenarios with a 90/10% energy distribution, where free cooling reaches 53 points.

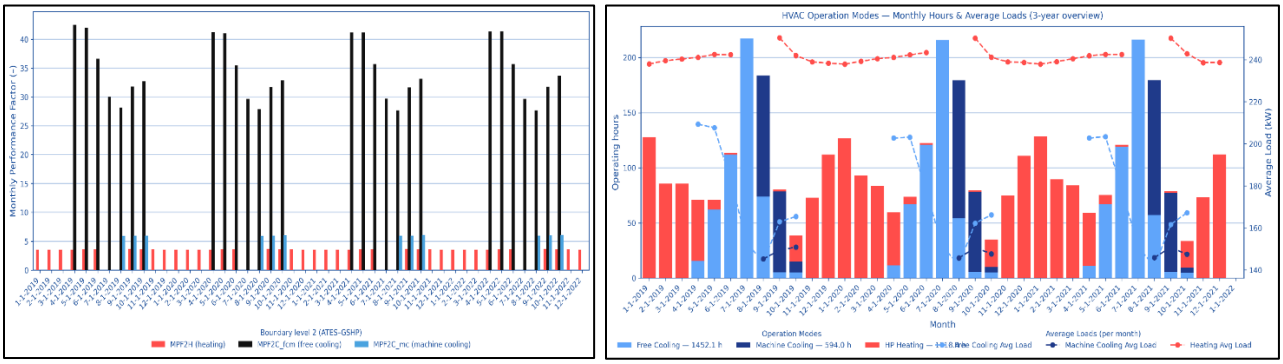

Figure 16: MPF for Boundary level 2, which accounts for both ATES and HP units and their respective circulation pumps for the constrained ATES with 60/40% energy distribution (left), and operating hours and heating-cooling power for each operating mode for the constrained ATES with 60/40% energy distribution (right).

The monthly operating hours of the heating system (left axis) and its average delivered power (right axis) are illustrated in Figure 16 (right). As in previous scenarios, the cooling power remains only a fraction of the heating power. The initial hypothesis attributed this discrepancy to the mass flow modulation implemented in the ATES. However, since this scenario includes machine cooling—where no modulation is applied, it is clear that additional factors are influencing the reduced power levels in both free cooling and machine cooling modes. These limitations are likely linked to characteristics of the model itself, and further analysis is needed to fully understand the underlying causes.

The case study presented by (Abuasbeh, 2021) provides a useful reference point, showing that the real system delivers higher cooling power than heating power. Although mean monthly values are not explicitly reported, the study presents binned outdoor temperatures alongside the corresponding power output and mean values for each bin. These results indicate that cooling powers can reach up to 200 kW (for a single building), whereas the simulated results in this work show values starting at around 140 kW at the beginning of the cooling season and decreasing to approximately 25 kW before machine cooling is activated towards the end of the season. It should also be noted that the values reported by (Abuasbeh, 2021) represent the combined operation of two buildings, while the present study models only a single building. Nevertheless, the discrepancy between the real and simulated results highlights the need for further investigation and model calibration to better capture the cooling performance of the system.

6.4 Scenario 4 constrained ATES 40/10%

The Building: Scenario 4 represents a constrained ATES and an optimal 90/10% HP to DH energy distribution. As seen in Figure 17 (left), the building's monthly operation results resemble those of Scenario 2, but with reduced machine cooling participation, which is only marginally present in September of the first simulated year.

The ATES: The ATES energy injection and extraction patterns are presented in Figure 17 (right). On initial observation, the injection and extraction values appear to be reasonably balanced. However, a more detailed analysis of the annual energy indicates that the hot well

is utilized to a greater extent than the cold well, resulting in an energy ratio of 0.8. This value is marginally higher than that observed in scenario 2, indicating a modest increase towards balanced well operation.

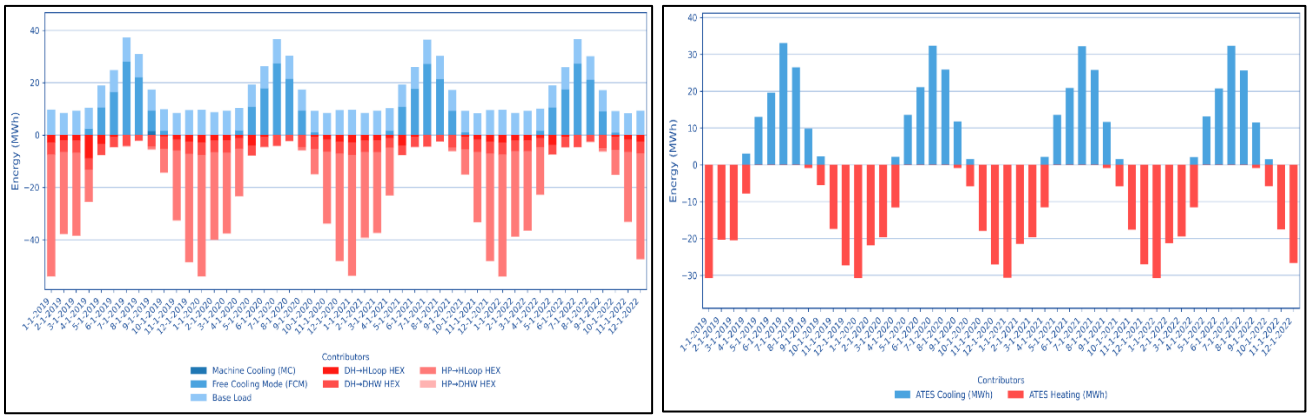

Figure 17: Building monthly cooling and heating loads by source for constrained ATES with 90/10% energy distribution (left). Monthly energy extracted and injected from the ATES [MWh] for cooling and heating. Scenario with a constrained aquifer and 90/10% energy distribution (right).

The volumetric performance of Figure 18 in Scenario 4 is very similar to Scenario 2 (which also has a balanced ATES), with the exception of a marginally improved cooling performance in terms of volume per unit of energy.

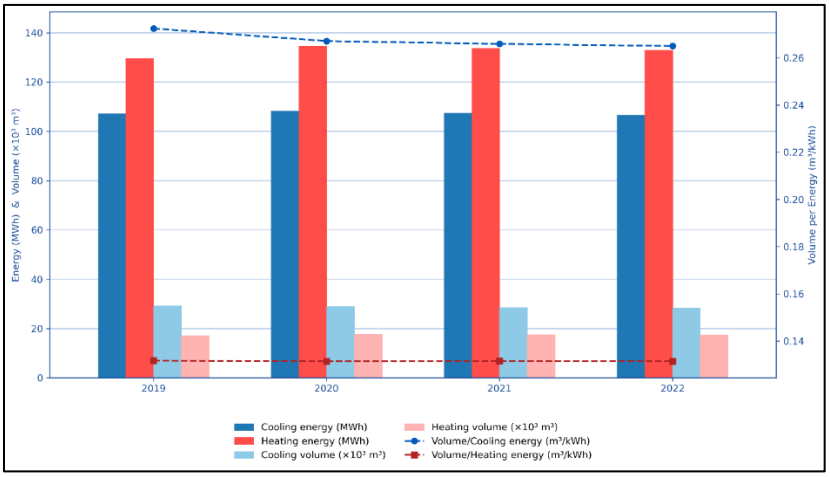

Figure 18: Total ATES yearly energy [MWh] and cooling/heating water volume [10e3 m3] (left axis) and volume per unit of energy [m3/kWh] (right axis) for constrained ATES with 90/10% energy distribution.

Figure 19 shows an ATES temperature distribution closely matching scenario 2: cold-well injection temperatures remain low, and cold-well extraction temperatures are lower than in scenarios 1 and 3. In the unbalanced cases (scenario 1 and scenario 3), cooling water drawn from the cold well spans roughly 5.8 °C to over 10 °C. By contrast, hot-well extraction and injection temperatures appear less sensitive to the ATES energy balance, where the only significant changes observed are in the minimum hot-well injection temperature. With injection values near 7 °C, whereas the unbalanced cases maintain a higher minimum near 10 °C.

KPI Evaluation: the global MPF2 that accounts for combined ATES+HP operations is presented in Figure 20 (left), where the cooling index is divided into free cooling, machine cooling, and a combined value that accounts for both cooling modes. The results are nearly identical to the MPF2 index presented in scenario 2, except for the small contribution of machine cooling. The cooling results are consistently 10 points above the unbalanced scenarios (scenario 1 and scenario 3), thereby emphasizing the energy-performance gains achieved when the system is operated in a more optimized, thermally balanced manner.

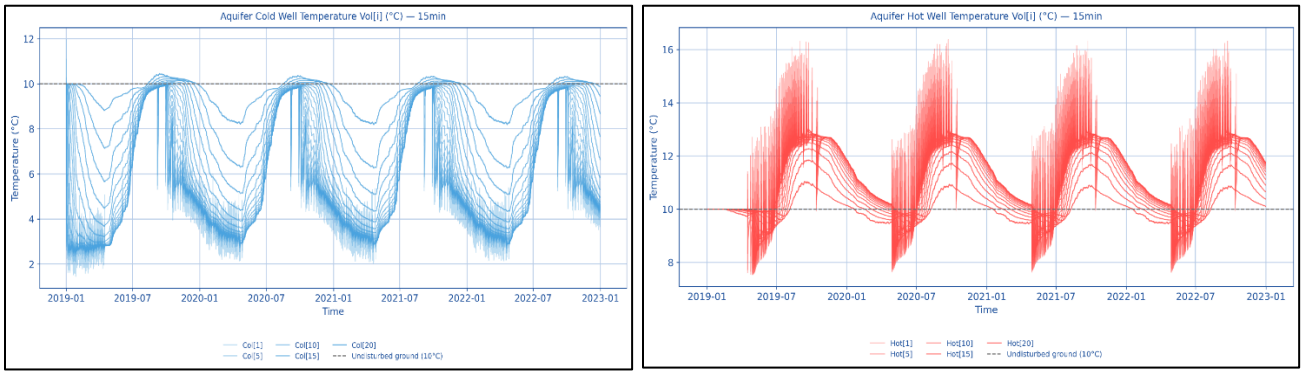

Figure 19: Aquifer water temperature distribution for each one of 20-control volume of the ATES modeled in Scenario 4. The cold well temperature distribution can be seen in (left), and the hot well temperature distribution is depicted in (right). Both plots consider 15-minute time series intervals.

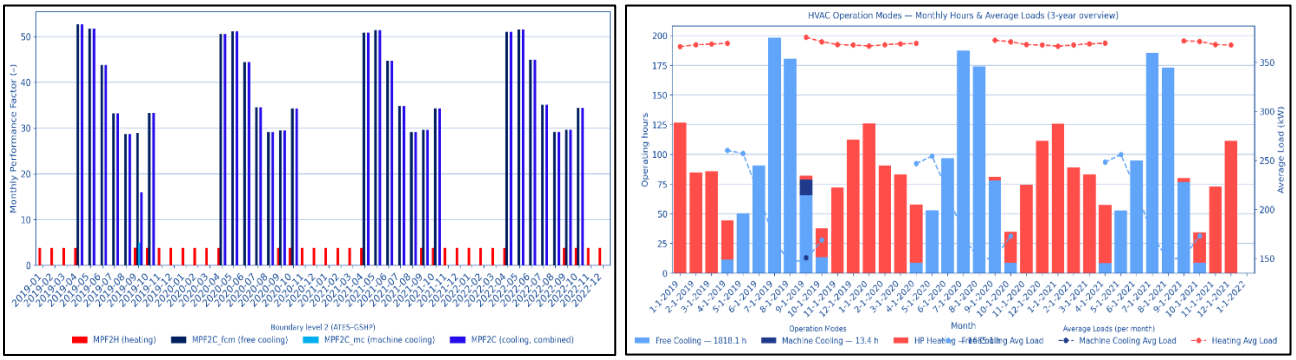

Figure 20: MPF for Boundary level 2, which accounts for both ATES and HP units and their respective circulation pumps for the constrained ATES with 90/10% energy distribution (left), and operating hours and heating-cooling power for each operating mode for the constrained ATES with 90/10% energy distribution (right).

Analogous to the MPF02 results, Figure 20 (right) presents the monthly operating hours and delivered power, revealing a very similar trend, with nearly identical values as scenario 2. This indicates that the imposed minimum and maximum extraction temperature limits have little influence on aquifer behavior in cases with high HP participation. These findings emphasize the importance of maximizing the energy contribution from the ATES during heating, as this approach would likely reduce overall reliance on district heating and, consequently, lower operating costs. Nevertheless, a detailed economic assessment is required to validate whether increased ATES participation in heating translates into lower total operating costs. Such an analysis should incorporate both fixed and variable operating costs, maintenance requirements, investment, depreciation, as well as seasonal energy pricing effects.

6.5 Heat Exchanger Performance KPI

Figure 21 presents the balance of the main heat-exchanger efficiencies (β_{HEX}) versus the sum of efficiencies, (σ_{HEX}) for the building as seen in equations (10) and (11) during heating (red) and cooling (blue). The markers distinguish between scenarios, and labels Y1–Y4 denote the simulation years 1–4. In this representation, β_{HEX} measures the balance between the two sides of the HEX (0 = balanced), while σ_{HEX} measures the combined effectiveness where$\sigma_{HEX} = 1.9$ represents the theoretical maximum for the model, given each individual side 0.95 maximum HEX effectiveness). All points lie slightly above zero for β_{HEX} axis (0.04–0.07), indicating a consistent but modest bias in favor of the building temperature difference. On the horizontal axis, values are close to the theoretical optimum ($\sigma_{HEX} \approx 1.77 - 1.82$), meaning the system achieves relatively high aggregate HEX effectiveness across the simulated years and operating modes.

When comparing scenarios, the 90/10% HP/DH split yields slightly better performance than the 60/40% energy split, obtaining high, σ_{HEX} and lower β_{HEX} i.e., more total effectiveness with a more balanced split between building and ATES. When assessing the yearly trend within each scenario, the constrained cases show a positive trend in cooling: Y1 to Y4 drift toward higher σ_{HEX} and a β_{HEX} closer to zero, as seen in 62 (annex), where a scaled version of Figure 2 is shown, suggesting an improving HEX operation trend for both 90/10% scenarios, and a declining σ_{HEX} trend for both 60/40% scenarios. This results in a more balanced use of available temperature on both sides when HP contribution is high. In contrast, the 60/40% the yearly trend remains roughly static or shows a deteriorating trend for σ_{HEX}.

Therefore, the operation is best when $\sigma_{HEX} \to 2$ and $\beta_{HEX} \to 0$ meaning large temperature differences on both sides are obtained. The four-scenario comparison shows that (i) the energy split between scenarios influences operation performance and (ii) constraint control helps cooling evolve toward a more optimal operation over time.

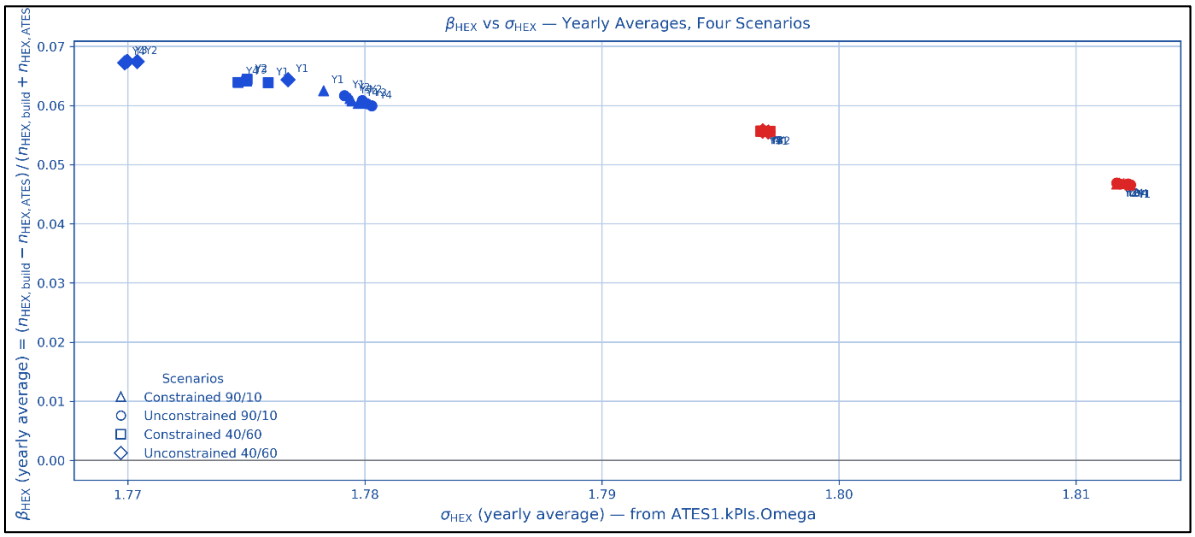

Figure 21: average yearly values for β_{HEX} and σ_{HEX} where the markers symbol identifies the 4 different scenarios with Y_i representing the simulated years accordingly.

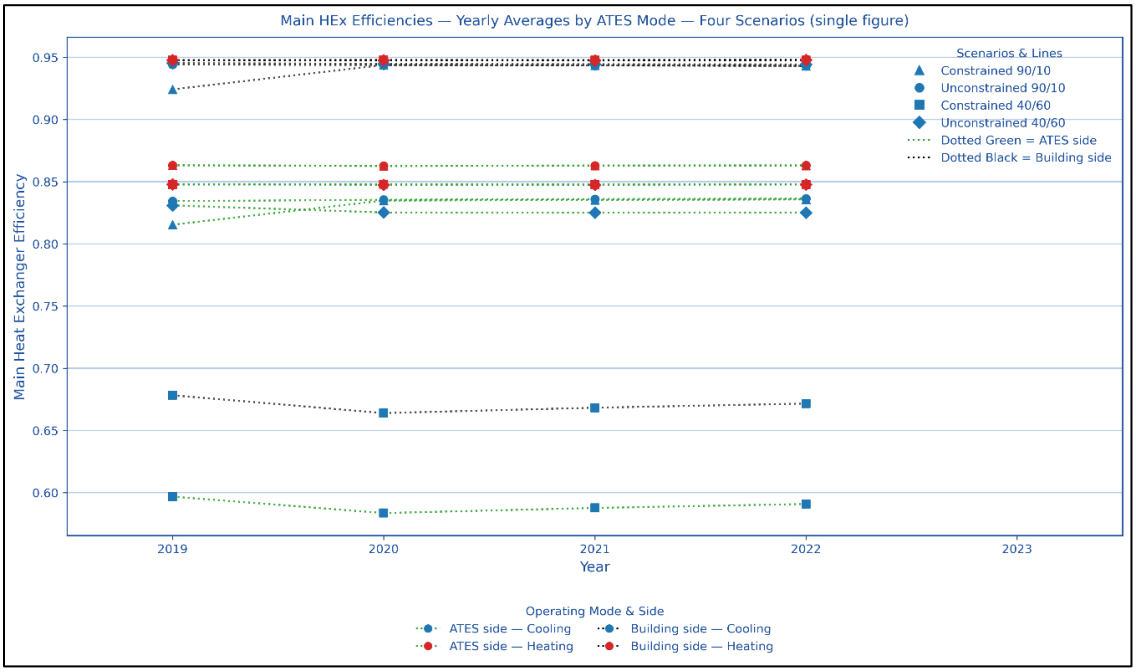

Figure 22: Heat exchanger efficiency (η_{HEX}) for the 4 modeled scenarios, in heating and cooling modes.

The heat exchanger efficiency (η_HEX) reflects the proportion of the maximum possible temperature difference that is effectively utilized across each heat exchanger. In general, the building side achieves consistently higher efficiencies than the ATES side, a trend also reported in previous case studies. This difference is likely influenced by modulation strategies applied to the ATES loop—implemented to ensure minimum extraction and injection levels—and by the slower response of the PI controller. These strategies help narrow the efficiency gap between the building and ATES sides, but also reduce flexibility in ATES-side operation. Ideally, both sides would operate with comparable efficiencies across all modes without compromising the system's thermal responsiveness.

When reviewing the independent heat exchangers' efficiencies (η_{HEX}) presented in Figure 22, the constrained 60/40% scenario displays the lowest performance with $\eta_{HEX-\text{ATES}} = 0.58$ and $\eta_{HEX-\text{Build}} = 0.67$. The remaining scenarios have similar results, with ATES heating efficiencies on average 0.03 points over the cooling values, and largely coincide (except for the constrained 60/40% scenario) in the buildings' side heating and cooling, where $\eta_{HEX-\text{Build}} \approx 0.95$.

7. CONCLUSIONS

This study evaluates the operation of a large-scale ATES-GSHP system for a commercial building, to optimize control strategies to improve overall energy performance and the temperature quality of the ATES. OMEdit was used to develop a model representing the system's components and capturing its dynamics. This work aims to shed light on how operational strategies and control decisions impact heat exchanger efficiencies, ATES balance, and the sustainability of the geothermal resource, aiming towards an optimized operation.

The simulations confirmed that the ATES can effectively shift seasonal loads and reduce reliance on district heating. Across the four simulated scenarios, the ATES supplied between 29–50% of the annual heating load and 41–57% of the annual space cooling demand. However, performance proved highly sensitive to the extraction/injection ratio. For example, the unconstrained 60/40% scenario resulted in an imbalance with an extracted-to-injected energy ratio of 0.74, leading to increases of 69% and 21% in the ATES volume per unit of energy used for heating and cooling, respectively, compared to the 90/10% scenarios. The effect is also noticeable in the MPF of the ATES, which is, on average, 10 points higher in both 90/10% scenarios than in the 60/40% cases. Free cooling MPFs vary between 55 and 26, highlighting the efficiency impacts on the ATES when operated in a balanced manner.

This shows the risks of a low HP energy contribution paired with a permissive extraction regime. The effect is also noticeable in the MPFs of the system (HP+ATES boundary), where both 90/10% scenarios have a free cooling MPF of 55 at the start of the cooling seasons, reducing to 25-30 at the end. Both 60/40% scenarios obtain, on average, 10 points under the 90/10% cases. This exposes the need to update current standards promoting efficient operation and HVAC system design.

When constraining the scenarios with low HP contribution (60%), a significant impact was observed when extraction temperatures were limited, reducing the average free cooling energy from the ATES by 28% and increasing the 4-year average extraction-to-injection ratio from 0.74 to nearly 1. On the other hand, when constraining the ATES with 90% of the heating energy provided by the HP, only a marginal effect was observed, slightly reducing the cooling load met by the ATES by 3% and lowering the energy ratio from 1.27 to 1.24. These results demonstrate that over-extracting energy from the ATES — i.e., withdrawing more heat for space heating than is reinjected during cooling — is more tolerable than over-injecting energy, where excessive heat is stored during cooling and not adequately recovered in the heating season.

System-level performance indicators also reflected these dynamics. The monthly performance factors (MPF2) in the model deviated from case study measurements, suggesting that calibration of hydraulic circuits and load profiles is necessary. Nevertheless, the results showed that mass flow modulation effectively increased heat exchanger effectiveness on the ATES side to as high as 0.95, the upper simulation limit, ensuring a higher quality of thermal exchange and mitigating risks of thermal breakthrough.

A key finding is that control strategies — such as extraction temperature thresholds, flow modulation, and operational mode switching between free and machine cooling — can be as critical as component efficiencies. For example, free cooling covered all cooling loads in the unconstrained scenarios, eliminating the need for mechanical cooling, while machine cooling became necessary under constrained ATES operation. This shows that smart operation not only balances the aquifer but also reduces electricity consumption and pumping energy (i.e., less volume required per unit of delivered cooling energy).

This study also suggests that GSHP–ATES integration can significantly lower reliance on district heating, reducing operating costs, especially when balanced operation is achieved (with extraction/injection ratio> 1.0), thus ensuring the long-term sustainability of the geothermal resource. Economic considerations remain crucial: district heating tariffs, fixed and variable electricity costs, and capital investments for additional components (e.g., DHW storage tanks) must be incorporated in future assessments.

Finally, future work should focus on improved calibration using detailed monitoring data from the Rosenborg case study, as well as the implementation of additional control and optimization strategies. Extending the model to multi-building operation (Hus 3 + Hus 4) and evaluating long-term thermal drift of the aquifer would provide deeper insights. Additional injection constraints are needed to limit the minimum cold well injection temperature, which reaches values of 2°C, which is too low and could affect geothermal hydro-chemical stability and operational problems. Introducing a domestic hot water storage tank could further increase heat pump coverage of DHW demand. Coupling the technical analysis with cost–benefit assessments will be essential for fully capturing the potential of GSHP–ATES systems as a sustainable alternative for large commercial buildings.

REFERENCES

Abuasbeh, M. (2021). Annex 52—Case study report for Rosenborg, Sweden. GSHP installation coupled with aquifer thermal energy storage ATES suppling heating and cooling for two commercial buildings. Heat Pump Centre. https://doi.org/10.23697/6H7V-BT33

Abuasbeh, M., Acuña, J., Lazzarotto, A., & Palm, B. (2021a). Long term performance monitoring and KPIs' evaluation of Aquifer Thermal Energy Storage system in Esker formation: Case study in Stockholm. Geothermics, 96, 102166. https://doi.org/10.1016/j.geothermics.2021.102166

Abuasbeh, M., Acuña, J., Lazzarotto, A., & Palm, B. (2021b). Long term performance monitoring and KPIs' evaluation of Aquifer Thermal Energy Storage system in Esker formation: Case study in Stockholm. Geothermics, 96, 102166. https://doi.org/10.1016/j.geothermics.2021.102166

Analysis of an integrated heating and cooling system for a building complex with focus on long–term thermal storage. (n.d.). CoLab. Retrieved January 31, 2026, from https://colab.ws/articles/10.1016%2Fj.applthermaleng.2018.09.044

Directorate-General for Communication (European Commission). (2021). Making our homes and buildings fit for a greener future. Publications Office of the European Union. https://data.europa.eu/doi/10.2775/25443

European Commission. (2021). Questions and Answers: Corporate Sustainability Reporting Directive proposal. https://ec.europa.eu/commission/presscorner/api/files/document/print/en/qanda_21_1806/QANDA_21_1806_EN.pdf

Hesaraki, A., Holmberg, S., & Haghighat, F. (2015). Seasonal thermal energy storage with heat pumps and low temperatures in building projects—A comparative review. Renewable and Sustainable Energy Reviews, 43, 1199–1213. https://doi.org/10.1016/j.rser.2014.12.002

Lyden, A., Brown, C. S., Kolo, I., Falcone, G., & Friedrich, D. (2022). Seasonal thermal energy storage in smart energy systems: District-level applications and modelling approaches. Renewable and Sustainable Energy Reviews, 167, 112760. https://doi.org/10.1016/j.rser.2022.112760

Modelica Buildings Library training at the American Modelica Conference. (n.d.). Retrieved January 31, 2026, from https://simulationresearch.lbl.gov/modelica/training/2024/10/14/training-american-modelica-conference.html

Schiera, D. S., Barbierato, L., Lanzini, A., Borchiellini, R., Pons, E., Bompard, E., Patti, E., Macii, E., & Bottaccioli, L. (2021). A Distributed Multimodel Platform to Cosimulate Multienergy Systems in Smart Buildings. IEEE Transactions on Industry Applications, 57(5), 4428–4440. https://doi.org/10.1109/TIA.2021.3094497

Spitler, J. D., Berglöf, K., Mazzotti Pallard, W., & Witte, H. (2021). IEA HPT Annex 52 - Long-term performance monitoring of GSHP systems for commercial, institutional and multifamily buildings: Guidelines for Calculation of Uncertainties. https://urn.kb.se/resolve?urn=urn:nbn:se:kth:diva-319584